

Alloying Element Vaporization and Weld Pool Temperature during Laser Welding of AISI 202 Stainless Steel

P. A. A. KHAN and T. DEBROY

Alloying element vaporization rates, plasma composition, and the changes in weld composition during laser welding of 202 stainless steel are discussed in this paper. Iron, manganese, and chromium were the most dominant species in the plasma. During laser welding it is always a difficult task to measure the temperature of the weld pool since this region is surrounded by hot plasma. In this paper a novel technique for the determination of weld pool temperature is presented. It is demonstrated that the relative rates of vaporization of any two elements from the molten pool can serve as an indicator of weld pool temperature, irrespective of the element pair selected. The composition of the solidified region calculated from the measured values of vaporization rate, plasma composition, and the volume of the solidified region was in good agreement with the weld composition determined by electron probe microanalysis technique.

I. INTRODUCTION

THE importance of element vaporization phenomena during laser welding process has been emphasized in recent studies.^{1,2,3} The vaporization process is particularly important in the laser welding of alloys containing one or more volatile components because of the potential loss of elements from the laser melted pools. The principal factors that govern the rates of vaporization of different elements are the temperature distribution at the surface of the molten pool and the composition of the melt. The temperature distribution, in turn, is governed by several factors including the rate of absorption of beam energy by the workpiece and convection in the molten region driven by surface tension gradients and the natural convection. The rate of absorption of the beam energy is dependent on the plasma composition which again is influenced by the temperature distribution at the surface of the molten pool.

The complexity in the understanding of the element vaporization process arises from the interdependence of various physical phenomena that are involved in the process. Because of these complexities, no basic formalism is available at present to predict either the composition or the temperature of the plasma. Even the measurement of pool temperature is a formidable task since the molten pool is surrounded by hot plasma. Calculation of the pool temperature distribution by mathematical modeling would require prescription of the energy density distribution at the surface of the molten pool. Since the extent of the attenuation of the beam energy in the vicinity of the molten zone is dependent on the amount and composition of the plasma, determination of the energy density distribution at the surface of the workpiece with a reasonable degree of trustworthiness is not a straightforward task. If approximate calculations of pool temperature are made with several simplifying assumptions, the predicted value of pool temperature must be compared with experimentally determined values to examine the reliability of the prediction scheme. Therefore, the need to obtain experimental data on the pool temperature and plasma composition cannot be overemphasized.

P. A. A. KHAN, Graduate Assistant, and T. DEBROY, Associate Professor of Metallurgy, are with the Department of Materials Science and Engineering, The Pennsylvania State University, University Park, PA 16802.

Manuscript submitted March 29, 1984.

In this paper a new technique for the determination of weld pool temperature is demonstrated. Experimental data on the alloying element vaporization rates, plasma composition, and the changes in the weld composition during laser welding of AISI 202 stainless steel are discussed.

II. EXPERIMENTAL PROCEDURES

A schematic diagram of the experimental set-up is presented in Figure 1. A carbon dioxide laser, Coherent Model Everlase 525-1, capable of producing a maximum output power of 575 watts in the continuous wave mode, was used. Samples were placed on a remotely controlled, electrically operated table capable of providing linear motion. All welding was carried out inside a plexiglas box using a 2.54×10^{-2} m diameter, 0.127 m focal length Zn-Se lens with an antireflection coating.

The total rate of alloying element vaporization was determined from the measured values of the loss in sample weight resulting from element vaporization and the laser material interaction time. The interaction time was recorded

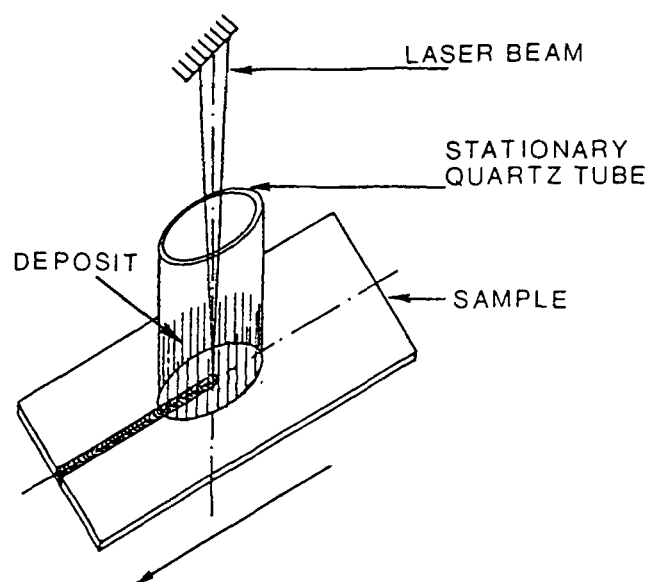


Fig. 1—A schematic diagram of the experimental set-up.

by an electronic chronometer suitably connected to the movable table to obtain automatic clock start and stop features. Samples of approximately 3.5×10^{-2} m length, 1.5×10^{-2} m width, and 0.07×10^{-2} m thickness were used for these experiments. Typical sample weight was about 2×10^{-3} kg. It may be of interest to note that in view of the small weight loss during welding, the weight loss measurements are best undertaken utilizing samples of small initial weights. Furthermore, to obtain precision in measurements, samples were irradiated several times along parallel paths so that the weight loss due to vaporization was significant.

A portion of the vaporized material was collected as condensation on the inner surface of a hollow, cylindrical, both end open quartz tube which was held stationary and co-axial with the laser beam. The composition of the condensate was determined by electron probe microanalysis (EPMA) technique. The EPMA was also used to determine the concentration profiles of various alloying elements in the weld zone and in the base metal.

The width and the cross-sectional area of the weld zone were determined at several locations along the length of the specimens by optical microscopy. The volume of the weld zone was determined from the average area of cross-section of the solidified zone and the length of the specimen.

III. RESULTS AND DISCUSSION

A. Vaporization Rates

For specimens irradiated at different laser powers, the measured rates of vaporization are plotted as a function of laser power in Figure 2. The increase in the overall vaporization rate with the increase in the laser power is due to two factors.^{4,5} First, the higher the laser power the higher the surface area of the molten zone where vaporization can occur. An idea of the surface area available for vaporization can be obtained from the width of the molten zone. The width of the solidified zone was measured along the length of the specimens by optical microscopy. The variation in the measured values was found to be within ± 5 pct throughout the entire length except near the ends where a slightly wider weld bead was observed due to end effects. The strong relationship between the area of molten pool and the laser

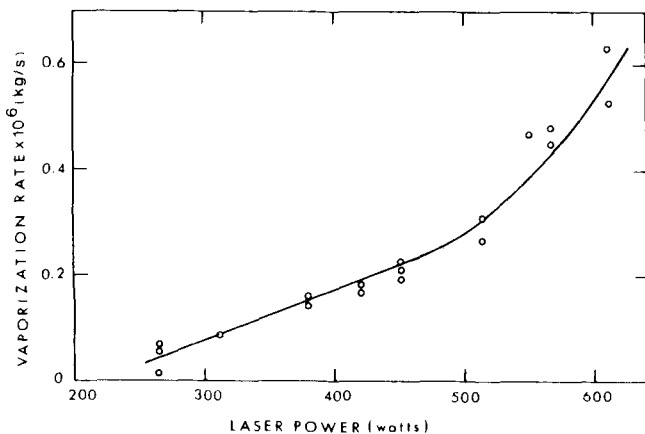


Fig. 2—Plot of measured vaporization rate vs laser power for AISI 202 stainless steel. Welding speed: 3.5×10^{-3} m/s, shielding gas flow rate: 1×10^{-4} m³/s.

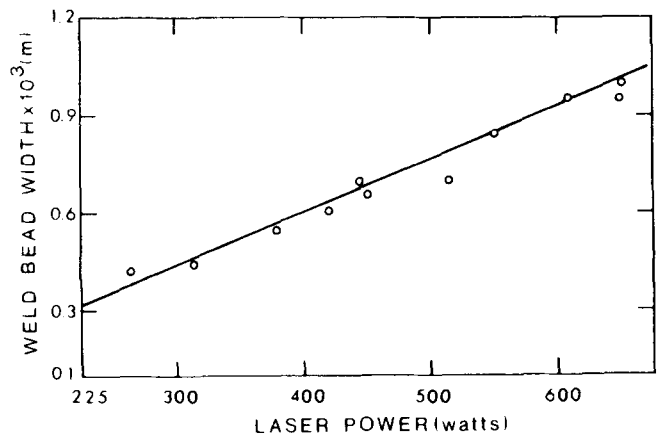


Fig. 3—Plot of weld bead width vs laser power for AISI 202 stainless steel. Welding speed: 3×10^{-3} m/s, shielding gas flow rate: 1×10^{-4} m³/s.

power is clearly evident in Figure 3 where the width of the weld bead is plotted as a function of laser power. Secondly, it is known that the rate of vaporization is a strong function of temperature. The high vaporization rate observed at high laser power is consistent with the fact that the weld pool temperature increases with the increase in laser power.

The weight loss measurements provide information about the overall vaporization rate. Vaporization of different elements from the molten zone occurs at different rates. These contributions have been measured by the analysis of the vapor deposited on the inner surface of a quartz tube. The relative quantities of different elements obtained from the analysis are presented in Table I. It is observed that iron, manganese, and chromium are the most dominant vapors in the plasma followed by Ni present at a low concentration. It will be shown subsequently that these compositions are also of significant value in the estimation of the weld pool temperature.

Table I. Relative Quantities of Different Elements (Moles of *i*/Moles of *j*) Present in the Plasma

Sample No.	n_{Fe}/n_{Mn}	n_{Cr}/n_{Mn}	n_{Ni}/n_{Mn}
1	1.09	0.58	0.04
2	1.16	0.58	0.07
3	1.14	0.51	0.06
4	1.01	0.50	0.04
5	1.03	0.50	0.05
6	1.07	0.52	0.05
7	1.16	0.72	0.06
8	1.06	0.67	0.06

Laser power = 560 watts
 Welding speed = 3.5×10^{-3} m/s
 Helium flow rate = 1.0×10^{-4} m³/s

B. Role of Liquid Phase Transport

In several systems the rate of vaporization is controlled by the transport of elements in the liquid phase.⁶ Therefore, it is necessary to examine the role of liquid phase transport in the vaporization of elements from laser melted pools.

Since iron is present at a very high concentration in the melt, it is unlikely that the transport of iron in the liquid phase controls its rate of vaporization. Furthermore, since the vaporization rates of iron and manganese are roughly

equal, it is unlikely that the transport of manganese in the liquid phase controls its rate of vaporization.

C. Selective Vaporization as an Indicator of Pool Temperature

The rates of vaporization of different elements at low pressure can be calculated from the relation:⁷

$$J_i = A_c P_i / \sqrt{2\pi M_i R T} \quad [1]$$

where J_i is the vaporization rate in kg-moles/m² s, A_c is a dimensionless parameter, P_i is the partial pressure of i in N/m², M_i is the molecular weight of i in kg/kg-mole, R is the gas constant in kg m²/(s² kg-mole K), and T is the temperature in K. Since A_c is not known, it is convenient to use the following dimensionless form of the above equation:

$$J_i/J_j = (P_i/P_j) (M_j/M_i)^{1/2} \quad [2]$$

The equilibrium partial pressure, P_i , of an element i over the molten pool depends upon the composition of the molten pool and temperature. The partial pressure values of different elements can be calculated from the thermodynamic data^{8,9} available in the literature. The values of the equilibrium partial pressures of different elements over liquid AISI 202 steel, calculated assuming ideal solution behavior at 2500 and 3000 K, are presented in Table II. It is observed from the calculated values that the extent of variation of the equilibrium partial pressures resulting from the change in temperature is different for different elements. Since the vaporization rates of the individual elements are proportional to their equilibrium partial pressures, the ratio of the vaporization rates of any two elements can be a strong function of temperature. Alternatively, for a given composition of the molten pool, if the ratio of the vaporization rates of two elements is known, the pool temperature can be determined.

The calculated values of partial pressures were used in Eq. [2] to calculate the ratio of the vaporization rates of Fe and Mn as a function of temperature. The calculated values of the ratio are plotted as a function of temperature in Figure 4. It is observed that the ratio of the rates is a strong function of temperature. If the experimentally determined value of J_{Fe}/J_{Mn} , presented in Table I, is utilized to determine the pool temperature from this figure, the temperature is found to be 3120 K. Since there may be a significant temperature gradient in the weld pool, the calculated temperature can be regarded as an effective vaporization temperature. Furthermore, since the vaporization rate increases strongly with the increase in temperature, the effective temperature may be expected to be close to the highest temperature value in the molten metal pool.

Table II. Partial Pressures of Alloying Elements over AISI 202 Stainless Steel

Element	Concentration (Wt Pct)	Temperature (K)	
		2500 (N/m ²)	3000 (N/m ²)
Fe	69.3	2106	35996
Mn	7.5	16932	54661
Cr	17.8	1466	25331
Ni	4.7	80	2527

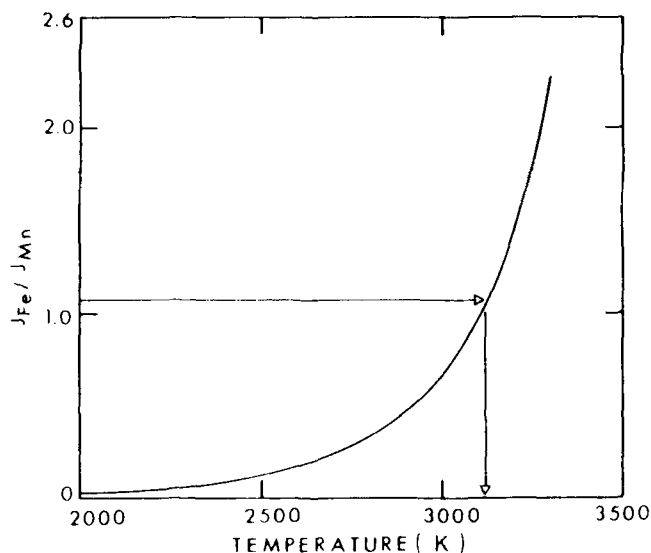


Fig. 4—The ratio of calculated vaporization rates of Fe and Mn, (J_{Fe}/J_{Mn}), as a function of temperature.

The computed flux ratio vs temperature plots for Cr-Mn and Ni-Mn are presented in Figure 5. Again, the measured values of the rates of vaporization of different element pairs, listed in Table I, were used for the calculation of pool temperature. The calculated values of pool temperature obtained from Figure 5 were 3050 K and 3110 K for the flux ratios of the binary pairs Cr-Mn and Ni-Mn, respectively. These values are in good agreement with the temperature calculated using the experimentally determined value of J_{Cr}/J_{Mn} . It is of interest to note that the selection of different element pairs leads to roughly similar values of the pool temperature.

The equilibrium partial pressures of different elements needed for the construction of Figures 4 and 5 were calculated assuming that the elements in the molten pool behave ideally. In view of the high weld pool temperature, it is anticipated that the ideal solution approach assumed for the calculations does not lead to significant inaccuracies. The values of the interaction parameters of different elements as a function of temperature are not available. However, calculations were also performed using the binary first order interaction parameter values at 1873 K available in the

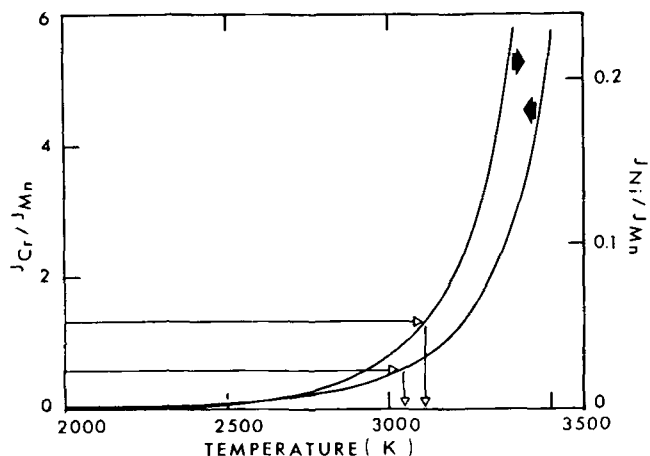


Fig. 5—The computed flux ratio vs temperature plots for Cr-Mn and Ni-Mn.

Table III. The Effective Weld Pool Temperature and Measured Composition Ratios of Alloying Elements Present in the Plasma

Composition Ratio (Moles of <i>i</i> /Moles of <i>j</i>)	Temperature (K)	
	Ideal	Non Ideal
$n_{Fe}/n_{Mn} = 1.08 \pm 0.07$	3120 ± 13	3190 ± 12
$n_{Cr}/n_{Mn} = 0.56 \pm 0.08$	3050 ± 40	3110 ± 33
$n_{Ni}/n_{Mn} = 0.05 \pm 0.01$	3110 ± 40	3240 ± 36
Average temperature	3093 ± 44	3180 ± 62

Table IV. Expected Change in the Weld Pool Composition

Element	Initial Composition (Wt Pct)	Expected Composition (Wt Pct)	Change in Composition (Wt Pct)
Fe	69.34	70.94	+ 1.6
Mn	7.48	5.68	- 1.8
Cr	17.85	17.75	- 0.1
Ni	4.72	4.82	+ 0.1

Volume of molten zone = $1.15 \times 10^{-8} \text{ m}^3$

Total weight loss = $4.5 \times 10^{-6} \text{ kg}$

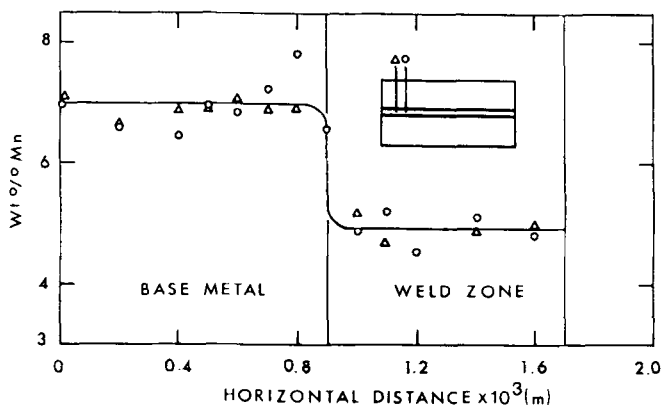


Fig. 6—Concentration profile of Mn in the weld zone and in the base metal at two different locations. The data represented by the triangles and circles were measured at $4 \times 10^{-3} \text{ m}$ and $7 \times 10^{-3} \text{ m}$, respectively, from the edge of the sample. Laser power: 560 watts, welding speed: $3.5 \times 10^{-3} \text{ m/s}$, shielding gas flow rate: $1 \times 10^{-4} \text{ m}^3/\text{s}$.

literature.⁹ It may be noted here that since the weld pool temperature is significantly higher than 1873 K, the actual deviation of the elements from ideal behavior would be much smaller than that predicted from the use of these interaction parameters. The effective pool temperature values obtained by considering both an ideal solution approach and a non-ideal solution approach are presented in Table III. It is observed that the weld pool temperatures estimated by using these two approaches are not significantly different.

D. Composition Changes in the Solidified Region

During the course of this investigation data were collected on (a) overall weight loss of the samples resulting from vaporization of elements, (b) composition of the vaporized material, and (c) volume of the solidified region. The composition of different elements in the solidified region can be easily calculated from these data by mass balances. The calculated changes in the composition of the solidified region are presented in Table IV. It is observed from the calculated values that the changes in the concentration of Fe, Ni, and Cr are relatively small. However, a significant

drop in manganese content from 7.48 wt pct to 5.68 wt pct is predicted. The measured concentration profiles of Mn in the weld zone and in the base metal at two different sections through the weld zone are presented in Figure 6. It is clear from this diagram that despite a small amount of scatter in the data, the concentration of Mn in the weld zone was lower than the corresponding concentration in the base metal by approximately 1.9 wt pct. The good agreement achieved between the calculated and the measured concentration demonstrates the consistency of the measured values of vaporization rate, composition of the vaporized material, dimensions of the solidified region, and the concentration profile measurements utilizing the electron probe micro-analysis technique.

IV. CONCLUSIONS

The principal conclusions from this work may be stated as follows:

1. During laser welding of AISI 202 stainless steels, the predominant species in the plasma are iron, manganese, and chromium.
2. The relative rates of vaporization of any two elements from the molten pool can serve as an indicator of the weld pool temperature. The calculated value of pool temperature was found to be independent of the element pair selected.
3. The manganese content of the weld zone was significantly lower than that in the base metal. The composition of the weld zone calculated from the measured values of vaporization rate, plasma composition, and the volume of the solidified region was in good agreement with the experimentally determined composition.

ACKNOWLEDGMENTS

The authors are pleased to acknowledge the financial support of this research by the United States Department of Energy, Office of Basic Energy Sciences under contract no. DE-AC02-83 ER 45030. The authors wish to thank Dr. Stanley Wolf of DOE for his interest in this work.

REFERENCES

1. A. Blake and J. Mazumder: "Control of Composition during Laser Welding of Aluminum-Magnesium Alloy Using a Plasma Suppression Technique," invited paper at ICALEO, Laser Institute of America, Toledo, OH, 1982.
2. A. Block-Bolten and T. W. Eagar: Proceedings of a Conference on "The Trends in the Welding Research in the U.S.," New Orleans, LA, ASM, Metals Park, OH, 1982.
3. L. R. Hetche, E. A. Metzbowler, J. D. Ayers, and P. G. Moore: *Naval Research Reviews*, 1981, vol. 28, pp. 4-20.
4. P. A. A. Khan: M. S. Thesis, The Pennsylvania State University, University Park, PA, 1983.
5. T. DebRoy: Final report submitted to The Engineering Foundation on Laser Welding of Ni-Cr-Mo Containing Steels, Department of Materials Science and Engineering, The Pennsylvania State University, University Park, PA, 1983.
6. G. H. Geiger and D. R. Poirier: *Transport Phenomena in Metallurgy*, Addison-Wesley Publishing Company, Reading, MA, 1973, pp. 563-67.
7. S. Dushman: *Scientific Foundations of Vacuum Technique*, John Wiley and Sons, Inc., New York, NY, 1949, pp. 18-24.
8. R. E. Honig and D. A. Kramer: *Physicochemical Measurements in Metal Research*, Interscience Publishers, New York, NY, 1970, vol. 4, pp. 505-17.
9. J. F. Elliott: *Electric Furnace Proceedings*, 1974, vol. 32, pp. 62-73.